2014 IEEE International Conference on Robotics & Automation (ICRA)
Hong Kong Convention and Exhibition Center
May 31 - June 7, 2014. Hong Kong, China

Extrinsic Calibration of 2D Laser Sensors

Dong-Geol Choi, Yunsu Bok, Jun-Sik Kim and In So Kweon

Abstract— **This paper describes a new methodology for estimating a relative pose of two 2D laser sensors. Two dimensional laser scan points do not have enough feature information for motion tracking. For this reason, additional image sensors or artificial landmarks have been used to find a relative pose. We propose the method to estimate a relative pose of 2D laser sensors without any additional sensor or artificial landmark. By scanning two orthogonal planes, we utilize only the coplanarity of the scan points on each plane and the orthogonality of the plane normals. Experiments with both synthetic and real data show the validity of the proposed method. To the best of our knowledge this works provides the first solution for the problem.**

I. INTRODUCTION

A laser range sensor has been one of the most important sensors in many robotic applications, mainly due to its accuracy and robustness at measuring distances. Wolf et al. [1] showed its usefulness for simultaneous localization and mapping (SLAM) successfully using one laser scanner in a 2D environment. With the evolution of robotic applications from two-dimensions to three-dimensions, demands to use range information in three dimensional applications have been growing. Many works [2] [3] [4] has been presented 6D SLAM using a camera and a laser range finder in an outdoor environment. An unmanned autonomous vehicle is usually equipped extraordinarily many sensors for such tasks. Thrun et al. [5] [6] successfully achieved important tasks such as vehicle motion estimation and target detection using several laser sensors, cameras and 3D sensors in the 2005 DARPA Grand Challenge and in the 2007 Urban Challenge. Bok et al. [7] showed large scale 3D reconstruction in an outdoor environment using 2 laser sensors and 2 cameras.

In these systems using multiple sensors, registration or extrinsic calibration of those sensors is critical, and thus, many efforts have been made for accurate registration between various sensors. However, there have been surprisingly few works on registering multiple laser range sensors. Because of the difficulties in searching for correspondences between scan data captured by moving laser range sensors, most of the previous approaches have utilized a camera attached to the set of laser scanners. Zhang et al. [8] used image sensors to calculate camera-laser extrinsic parameters when a planar calibration pattern was posed in the views of both the camera and the laser range sensor. Geo et al. and Underwood et al. [9] [10] proposed extrinsic calibration methods using artificial landmarks. The artificial landmarks with different reflectance are attached at known positions so that a user can determine the exact pose between the laser sensors and the mobile platform. Maddern et al. [11] proposed extrinsic calibration between 2D and 3D LIDAR sensors with respect to a vehicle base frame. Levinson et al. [12] used surface normals generated from local neighborhoods to find extrinsic and intrinsic calibration parameters for a Velodyne HDL-64E on a moving vehicle platform. All of these methods require complicated steps for calibration (eg. laser-camera-laser), or specially designed landmarks for laser-laser calibration. A 3D laser scanner is too expensive to be easily used for calibration.

We propose a new method for registering two laser scanners without any extra sensor or known motion information. The proposed method uses only scan data on two orthogonal planes. At each scan, each plane has two scan lines from the two laser scanners, and the coplanarity of the scan points provides a linear constraint to an unknown vector composed by the extrinsic parameters. The extrinsic parameters are extracted from the unknown vector using orthogonality between the two planes. Finally, we apply a nonlinear optimization based on those two scene constraints, coplanarity and orthogonality, to refine the solution.

II. EXTRINSIC CALIBRATION OF TWO SINGLE LINE LASER SENSORS

This section provides how to solve for the extrinsic parameters between two 2D laser sensors. We will derive a linear constraint on the relative pose between two laser sensors, and explain how to extract physically meaningful relative poses from the linearly constrained solutions. Refinement of the solution with nonlinear optimization will also be discussed in this section.

Assume that we have two laser range finders L_1 and L_2, and a plane Π_1 as shown in Fig. 1 (b). Each laser scan plane intersects Π_1 and for L_1, there are two points $\mathbf{q_1}$ and $\mathbf{q_2}$ defining the intersecting line in 3D. Similarly, for L_2, we can define two points $\mathbf{q_3}$ and $\mathbf{q_4}$. Note that all the points are represented in a common coordinate system, which is the coordinate system of L_1. The points represented in the coordinate system of L_1 and those in L_2 coordinate system will be denoted by $\mathbf{q_n} = [x_n\ y_n\ z_n]^\top$ and $\mathbf{q'_n} = [x'_n\ y'_n\ z'_n]^\top$,

This work was supported by the National Research Foundation of Korea(NRF) grant funded by the Korea government(MSIP) (No. 2010-0028680) and the National Research Foundation, Korea, under the NRF-ANR joint research program (No. 2011-0031920).

D.-G. Choi is a Ph.D. student of the Robotics Program, KAIST, Daejeon, Korea dgchoi@rcv.kaist.ac.kr

Y. Bok is a research assistant professor of Division of Future Vehicle, KAIST, Daejeon, Korea ysbok@rcv.kaist.ac.kr

J.-S. Kim is with Interaction and Robotics Research Center, Korea Institute of Science and Technology, Hwarangno 14-gil 5, Seongbuk-gu, Seoul, Korea junsik.kim@kist.re.kr

I. S. Kweon is a professor of Department of Electrical Engineering, KAIST, Daejeon, Korea iskweon@kaist.ac.kr

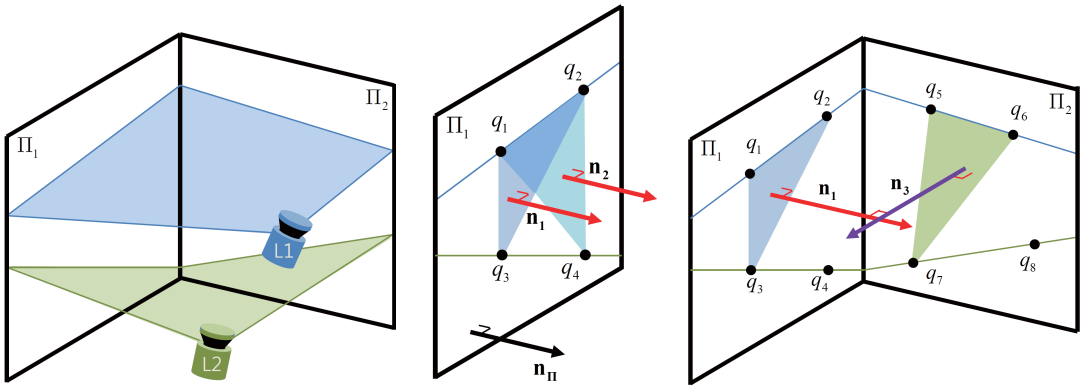

(a) System overview (b) Coplanarity (c) Orthogonality

Fig. 1: Proposed calibration setup and constraints for two laser sensors using two planes. (a) At each scan, each plane has two scan lines from the two laser scanners. (b) The coplanarity of the scan points provides a linear constraint to the unknown vector composed by the extrinsic parameters. (c) The extrinsic parameters are extracted from the linear system solution by using orthogonality between the two planes.

respectively. They can be transformed as

$$\mathbf{q_n} = \mathbf{R}\mathbf{q'_n} + \mathbf{t}. \tag{1}$$

where $\mathbf{R}$ and $\mathbf{t}$ are a rotation matrix and a translation vector that transforms points in L_2 coordinate to L_1 coordinate. The element of $\mathbf{R}$ at the i-th row and the j-th column is denoted by r_{ij}, and let $\mathbf{t} = [t_x \ t_y \ t_z]^\top$. Difference between two points will also be denoted by $\Delta\mathbf{q_{ij}} = \mathbf{q_i} - \mathbf{q_j} = [\Delta x_{ij} \ \Delta y_{ij} \ \Delta z_{ij}]^\top$ and $\Delta\mathbf{q'_{ij}} = \mathbf{q'_i} - \mathbf{q'_j} = [\Delta x'_{ij} \ \Delta y'_{ij} \ \Delta z'_{ij}]^\top$.

Fig. 1 (a) shows the overview of the proposed calibration method. We use the coplanarity and orthogonality between the two orthogonal planes to estimate extrinsic parameters.

A. Linear constraint using coplanarity

The normal vector $\mathbf{n}_\Pi$ of the plane Π_1 is represented with three points $\mathbf{q_1}$, $\mathbf{q_2}$ and $\mathbf{q_3}$ as

$$\mathbf{n}_\Pi \sim \mathbf{n_1} = (\mathbf{q_2} - \mathbf{q_1}) \times (\mathbf{q_3} - \mathbf{q_1}) \tag{2}$$

and with $\mathbf{q_1}$, $\mathbf{q_2}$ and $\mathbf{q_4}$,

$$\mathbf{n}_\Pi \sim \mathbf{n_2} = (\mathbf{q_2} - \mathbf{q_1}) \times (\mathbf{q_4} - \mathbf{q_1}). \tag{3}$$

Those two normal vectors $\mathbf{n_1}$ and $\mathbf{n_2}$ should be parallel, and it gives

$$((\mathbf{q_2} - \mathbf{q_1}) \times (\mathbf{q_3} - \mathbf{q_1})) \times ((\mathbf{q_2} - \mathbf{q_1}) \times (\mathbf{q_4} - \mathbf{q_1})) = \mathbf{0}. \tag{4}$$

The fact that $\Delta\mathbf{q_{21}} = (\mathbf{q_2} - \mathbf{q_1}) \neq 0$ makes (4) as

$$\Delta\mathbf{q_{21}} \cdot ((\mathbf{q_3} - \mathbf{q_1}) \times (\mathbf{q_4} - \mathbf{q_1})) = 0, \tag{5}$$

which means that $(\mathbf{q_3} - \mathbf{q_1}) \times (\mathbf{q_4} - \mathbf{q_1})$ is orthogonal to $\Delta\mathbf{q_{21}}$, geometrically.

Expansion of the second part $(\mathbf{q_3} - \mathbf{q_1}) \times (\mathbf{q_4} - \mathbf{q_1})$ is

$$\mathbf{q_3} \times \mathbf{q_4} - \mathbf{q_3} \times \mathbf{q_1} - \mathbf{q_1} \times \mathbf{q_4} + \mathbf{q_1} \times \mathbf{q_1}. \tag{6}$$

The point $\mathbf{q_3}$ is equal to $\mathbf{R}\mathbf{q'_3} + \mathbf{t}$, where $\mathbf{q'_3}$ is represented in the L_2 local coordinate system as mentioned above. The first term is expanded as

$$\begin{aligned} \mathbf{q_3} \times \mathbf{q_4} &= (\mathbf{R}\mathbf{q'_3} + \mathbf{t}) \times (\mathbf{R}\mathbf{q'_4} + \mathbf{t}) \\ &= \mathbf{R}(\mathbf{q'_3} \times \mathbf{q'_4}) + \mathbf{t} \times \mathbf{R}\Delta\mathbf{q'_{43}} \end{aligned} \tag{7}$$

The very next two terms are

$$-\mathbf{q_3} \times \mathbf{q_1} - \mathbf{q_1} \times \mathbf{q_4} = -\mathbf{q_1} \times \mathbf{R}\Delta\mathbf{q'_{43}}. \tag{8}$$

The last term $\mathbf{q_1} \times \mathbf{q_1}$ diminishes obviously, and (5) becomes,

$$\Delta\mathbf{q_{21}} \cdot (\mathbf{R}(\mathbf{q'_3} \times \mathbf{q'_4}) + (\mathbf{t} - \mathbf{q_1}) \times \mathbf{R}\Delta\mathbf{q'_{43}}) = 0 \tag{9}$$

Equation (9) is expanded as

$$\begin{bmatrix} \Delta x_{21}(z'_3x'_4 - x'_3z'_4) \\ \Delta x'_{43}(z_1x_2 - x_1z_2) \\ \Delta z'_{43}(z_1x_2 - x_1z_2) \\ \Delta z_{21}(z'_3x'_4 - x'_3z'_4) \\ \Delta x_{21}\Delta x'_{43} \\ \Delta x_{21}\Delta z'_{43} \\ \Delta z_{21}\Delta x'_{43} \\ \Delta z_{21}\Delta z'_{43} \end{bmatrix}^\top \begin{bmatrix} r_{12} \\ r_{21} \\ r_{23} \\ r_{32} \\ r_{31}t_y - r_{21}t_z \\ r_{33}t_y - r_{23}t_z \\ r_{21}t_x - r_{11}t_y \\ r_{23}t_x - r_{13}t_y \end{bmatrix} = 0, \tag{10}$$

which is a linear constraint equation on the extrinsic parameters $\mathbf{R}$ and $\mathbf{t}$. By stacking measurement vectors, a linear system $\mathbf{A}\mathbf{x} = \mathbf{0}$ is built.

At least seven frames (sets of concurrent scan data) are required to solve the equation via singular value decomposition (SVD). Let $\mathbf{v}$ be the right singular vector corresponding to the smallest singular value, and let v_i be the i-th element of $\mathbf{v}$. The solution $\mathbf{v}$ is obtained up to scale: the final solution is $\lambda\mathbf{v}$ with an unknown scale factor λ. Now, the remaining problems are two-folds: 1) determining the true scale λ, and 2) extracting the valid relative transformation $\mathbf{R}$ and $\mathbf{t}$ from the vector $\lambda\mathbf{v}$.

B. Pose parameters from the least square solution

The solution vector $\lambda\mathbf{v}$ is composed of the pose parameters $\mathbf{R}$ and $\mathbf{t}$ as shown in (10), and we extract the parameters from $\mathbf{v}$ and from additional constraints. From the orthonormality of R, $r_{12}^2+r_{22}^2+r_{32}^2=1$ and it gives the following equations from the form of the vector $\lambda\mathbf{v}$.

$$r_{22}(\lambda) = \pm\sqrt{1-\lambda^2 k_0} \tag{11}$$

$$v_1^2 + v_4^2 = v_2^2 + v_3^2 \tag{12}$$

$$v_4(v_3v_5 - v_2v_6) = v_1(v_3v_7 - v_2v_8) \tag{13}$$

Parameters k_n are known constants determined by the vector $\mathbf{v}$. From (10), (12), and (13), the rotation matrix $\mathbf{R}$ is expressed as a function of λ as

$$\mathbf{R}(\lambda) = \begin{bmatrix} -k_5 r_{22}(\lambda) \pm k_6 & \lambda k_1 & -k_8 r_{22}(\lambda) \mp k_7 \\ \lambda k_2 & r_{22}(\lambda) & \lambda k_3 \\ -k_7 r_{22}(\lambda) \mp k_8 & \lambda k_4 & -k_6 r_{22}(\lambda) \pm k_5 \end{bmatrix} \tag{14}$$

$$\mathbf{t}(\lambda) = \begin{bmatrix} \mp k_{12} r_{22}(\lambda) + k_{13} \\ \mp \lambda k_9 \\ \pm k_{10} r_{22}(\lambda) - k_{11} \end{bmatrix} \tag{15}$$

Equations (14) and (15), show that the extrinsic parameters $\mathbf{R}$ and $\mathbf{t}$ are finally expressed as functions of λ. The definitions of the constant k_n are given in the Appendix.

C. Scale candidates using orthogonality

An additional equation is required to determine the scale λ. In this paper, we utilize a pair of perpendicular planes. Scan data on both planes can be used to compute $\mathbf{v}$ because they share common $\mathbf{R}$ and $\mathbf{t}$. Normal vectors of the planes are functions of λ. The scale is determined using the orthogonal property of the vectors. Let $\mathbf{n_1}$ and $\mathbf{n_3}$ be the normal vectors of two orthogonal planes Π_1 and Π_2, respectively as shown in Fig. 1 (c).

Scanning the two planes, two lines can be extracted from range data. Lines on planes Π_1 and Π_2 scanned by L_1 are defined by $(\mathbf{q_1}, \mathbf{q_2})$ and $(\mathbf{q_5}, \mathbf{q_6})$, and those scanned by L_2 are defined by $(\mathbf{q_3}, \mathbf{q_4})$ and $(\mathbf{q_7}, \mathbf{q_8})$, respectively, as shown in Fig. 1 (c). Normal vectors $\mathbf{n}_1$ and $\mathbf{n}_3$ are computed using these points. The constants k_n from $\mathbf{v}$ are derived by tedious manipulations, whose details appear in the Appendix.

$$\mathbf{n_1} = \Delta\mathbf{q_{21}} \times \Delta\mathbf{q_{31}} = \begin{bmatrix} \lambda k_{14} \\ k_{15} r_{22}(\lambda) + k_{16} \\ \lambda k_{17} \end{bmatrix} \tag{16}$$

$$\mathbf{n_3} = \Delta\mathbf{q_{65}} \times \Delta\mathbf{q_{75}} = \begin{bmatrix} \lambda k_{18} \\ k_{19} r_{22}(\lambda) + k_{20} \\ \lambda k_{21} \end{bmatrix} \tag{17}$$

The dot product of the two normal vectors $\mathbf{n_1}$ and $\mathbf{n_3}$ must be equal to zero.

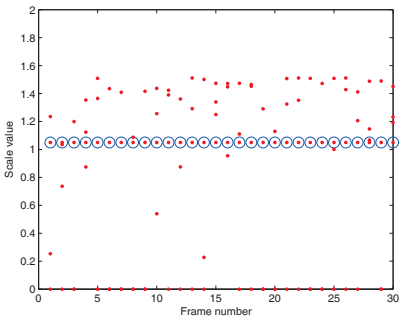

Fig. 2: Scale candidate values for all frames. Red dots denote scale candidates from each pair of orthogonal planes and blue circles the ground truth scale value.

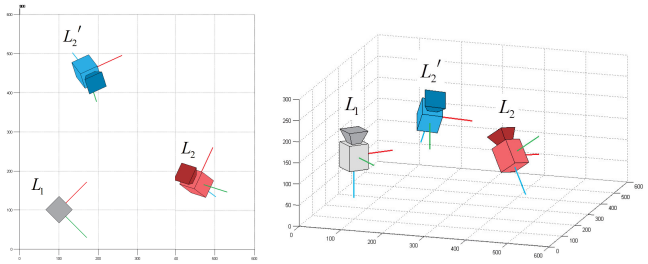

(a) Top view (b) Side view

Fig. 3: Sensor configurations using the true scale value and its 'mirrored' scale value (a) top view and (b) side view.

$$\begin{aligned} \mathbf{n_1} \cdot \mathbf{n_3} &= \begin{bmatrix} \lambda k_{14} \\ k_{15} r_{22}(\lambda) + k_{16} \\ \lambda k_{17} \end{bmatrix} \cdot \begin{bmatrix} \lambda k_{18} \\ k_{19} r_{22}(\lambda) + k_{20} \\ \lambda k_{21} \end{bmatrix} \\ &= k_{22}\lambda^2 + k_{23} r_{22}(\lambda) + k_{24} \\ &= k_{22}\lambda^2 \pm k_{23}(\sqrt{-\lambda^2 k_0 + 1}) + k_{24} \end{aligned} \tag{18}$$

Substituting the third term and computing the squares of both sides, we obtain

$$k_{22}^2\lambda^4 + (2k_{22}k_{24} + k_{23}^2 k_0)\lambda^2 - k_{23}^2 + k_{24}^2 = 0 \tag{19}$$

which is a special form of a 4-th order polynomial equation of λ. The candidates of the scale λ are computed by substituting $\mu = \lambda^2$, solving a quadratic equation and selecting positive solutions for μ. Equation (19) is a quadratic form and its coefficients contain double signs in the same order. Therefore we can obtain up to eight candidates for the scale per frame. The definitions of the constants k_n are provided in the Appendix.

D. Scale selection

As shown in Sect. II-C, each pair of orthogonal planes yields 8 solutions. Fig. 2 shows positive real scale values among all candidates. To find a unique solution, each one is verified using the equations derived from the other frames. In an ideal case, the equations must be equal to zero if the right solution is adopted. We select one candidate for each

frame which minimizes the equation evaluation values. The final solution for the scale is determined using a Gaussian kernel density estimation. Since the scale λ is substituted by $\mu = \lambda^2$, both signs of the final solution satisfy (19). The other solution with the opposite sign is referred to as a 'mirrored scale value' in the rest of this paper. Fig. 3 shows an example of two different sensor configurations derived from the solution pair. Gray and red lasers indicate L_1 and L_2, respectively. The solution using the mirrored scale value is displayed in blue denoted by L_2'. All sensors are transformed into the coordinate system of L_1. L_2 and L_2' are placed symmetrically from L_1. Both of the configurations satisfy all of the constraints proposed, and thus, it is not possible to choose the right solution between them. However, it is trivial to choose the right one by comparing them to the actual sensor configuration, because those two possible poses have different signs in translation with respect to L_1.

E. Nonlinear optimization

The initial solution computed in Sect. II-D is refined via non-linear optimization. We assumed that the two planes are perpendicular to each other in Sect. II-C. However, planes in real environments usually do not satisfy the assumption perfectly. We include the angle between the planes as an unknown parameter with an initial value of 90 degrees. Moreover, we estimate the pose of the sensor rig in each frame with respect to the planes in the optimization. Initial values of the pose for each frame must be computed first.

The pose of the sensor rig with respect to the planes has five degrees of freedom because the translation along an intersection line of the two planes cannot be estimated (i.e., translation vector has two degrees of freedom). Without loss of generality, we set the intersection line of the two planes as y-axis (i.e., the both planes contain the y-axis), and the normal vector $\mathbf{n_1}$ of Π_1 as x-axis of the world coordinate system. For each frame, scan data of L_2 are transformed into L_1 coordinate system and the normal vectors $\mathbf{n_1}$ and $\mathbf{n_3}$ of the two planes are computed by plane fitting. Since the normal vectors are computed up to scale, we fix their directions so that the signs of $\mathbf{n_1}\cdot(\mathbf{q_6}-\mathbf{q_5})$ and $\mathbf{n_3}\cdot(\mathbf{q_1}-\mathbf{q_2})$ are must be positive, when the scanned surfaces are concave. (see Fig. 1(c)). After computing the normal vectors and their directions, we set three orthonormal vectors $\mathbf{v_x}$, $\mathbf{v_y}$ and $\mathbf{v_z}$ which correspond to x, y and z axes of the world coordinate system.

$$\mathbf{v_x} = \frac{\mathbf{n_1}}{\|\mathbf{n_1}\|} \tag{20}$$

$$\mathbf{v_y} = \frac{\mathbf{n_3} \times \mathbf{n_1}}{\|\mathbf{n_3} \times \mathbf{n_1}\|} \tag{21}$$

$$\mathbf{v_z} = \mathbf{v_x} \times \mathbf{v_y} \tag{22}$$

Rotation part $\hat{\mathbf{R}}_\mathbf{i}$ of the transformation from L_1 to the world coordinate in i-th scan data frame is computed as

$$\hat{\mathbf{R}}_\mathbf{i} = \begin{bmatrix} \mathbf{v_x} & \mathbf{v_y} & \mathbf{v_z} \end{bmatrix}^\top. \tag{23}$$

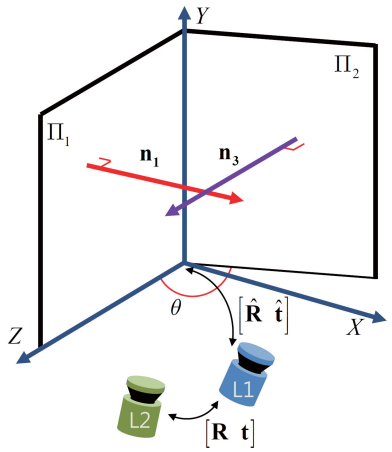

Fig. 4: Definition of two planes in the world coordinate system. The intersecting line of the planes is set as y-axis. The normal vector $\mathbf{n_1}$ of Π_1 is set as x-axis. The normal vector $\mathbf{n_3}$ of Π_2 is a function of θ, the angle between two planes.

We have mentioned that the translation vector $\hat{\mathbf{t}}_\mathbf{i}$ has only two degrees of freedom. Since we set the intersection line as y-axis, y element of the translation can be any value. Without loss of generality, we set its value to zero. The other elements are computed transforming the intersecting point $\mathbf{q_{int}}$ of the two lines $\overline{\mathbf{q_1 q_2}}$ and $\overline{\mathbf{q_5 q_6}}$ into the world coordinate system using the fact that $\mathbf{q_{int}}$ must lie on the y-axis.

$$\mathbf{q_{int}} \sim (\mathbf{q_1} \times \mathbf{q_2}) \times (\mathbf{q_5} \times \mathbf{q_6}) \tag{24}$$

$$\hat{\mathbf{t}}_\mathbf{i} = \begin{bmatrix} -\mathbf{v_x}^\top \mathbf{q_{int}} & 0 & -\mathbf{v_z}^\top \mathbf{q_{int}} \end{bmatrix}^\top \tag{25}$$

In the optimization process, the angle θ between the two planes affects their normal vectors. In our implementation, we fix $\hat{\mathbf{n}}_\mathbf{1}$ equal to x-axis and adjust $\hat{\mathbf{n}}_\mathbf{3}$ using (27) (see Fig. 4).

$$\hat{\mathbf{n}}_\mathbf{1} = \begin{bmatrix} 1 & 0 & 0 \end{bmatrix}^\top \tag{26}$$

$$\hat{\mathbf{n}}_\mathbf{3} = \begin{bmatrix} \cos\theta & 0 & \sin\theta \end{bmatrix}^\top \tag{27}$$

The cost function f for optimization is the squared sum of the Euclidean distances between the two planes and the scan data in the world coordinate system. Constant terms of the planes are equal to zero because the origin of the world coordinate system is on both planes. n is the number of scan data frame that used in the optimization. Note that $\hat{\mathbf{n}}_\mathbf{3}$ is a function of θ, as shown in (27).

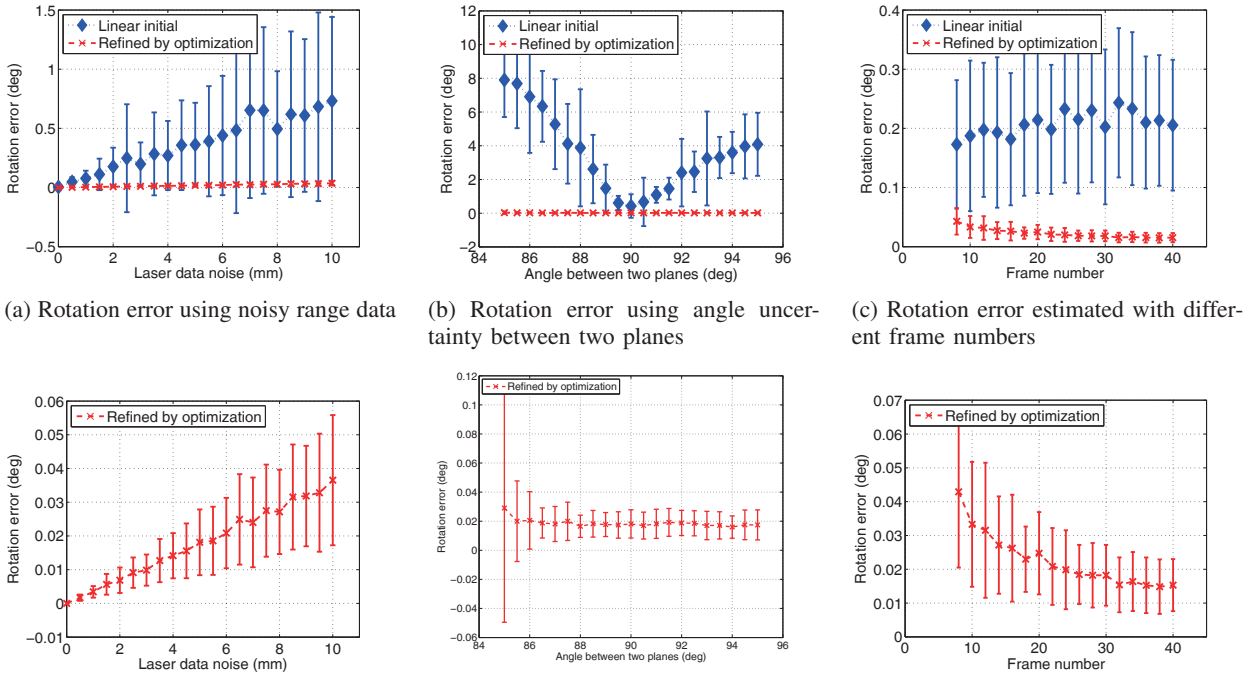

(a) Rotation error using noisy range data

(b) Rotation error using angle uncertainty between two planes

(c) Rotation error estimated with different frame numbers

(d) Rotation error using noisy range data

(e) Rotation error using angle uncertainty between two planes

(f) Rotation error estimated with different frame numbers

Fig. 5: Performance analysis of initial results (blue) and refined results (red) from three aspects: (a, d) measurement noise, (b, e) errors in the orthogonality assumption, and (c, f) the number of frames used in the estimation. (a, b and c) are shown comparision results between the initial and refined results. (d, e and f) show more details of the performance after the refinement.

$$
\begin{aligned}
f(\mathbf{R},\mathbf{t},\hat{\mathbf{R}}_\mathbf{i},\hat{\mathbf{t}}_\mathbf{i},\theta) = \sum_{\mathbf{i=1}}^{n}\Big(& \sum_{\mathbf{q}\in(L_1,\Pi_1)} (\hat{\mathbf{n}}_\mathbf{1}^\top(\hat{\mathbf{R}}_\mathbf{i}\mathbf{q}+\hat{\mathbf{t}}_\mathbf{i}))^2 \\
& + \sum_{\mathbf{q}\in(L_1,\Pi_2)} (\hat{\mathbf{n}}_\mathbf{3}^\top(\hat{\mathbf{R}}_\mathbf{i}\mathbf{q}+\hat{\mathbf{t}}_\mathbf{i}))^2 \\
& + \sum_{\mathbf{q'}\in(L_2,\Pi_1)} (\hat{\mathbf{n}}_\mathbf{1}^\top(\hat{\mathbf{R}}_\mathbf{i}(\mathbf{R}\mathbf{q'}+\mathbf{t})+\hat{\mathbf{t}}_\mathbf{i}))^2 \\
& + \sum_{\mathbf{q'}\in(L_2,\Pi_2)} (\hat{\mathbf{n}}_\mathbf{3}^\top(\hat{\mathbf{R}}_\mathbf{i}(\mathbf{R}\mathbf{q'}+\mathbf{t})+\hat{\mathbf{t}}_\mathbf{i}))^2\Big)
\end{aligned}
\tag{28}
$$

III. EXPERIMENTAL RESULTS

A. Simulation using synthetic data

We generated a set of synthetic data to verify the performance of the proposed algorithm. The two planes in the world coordinate system $\mathbf{x} = 0$ and $\mathbf{z} = 0$ were used as orthogonal planes scanned by laser sensors. The positions of the two sensors are generated randomly within 100< t_x <500, -500< t_y <500 and 100< t_z <500, and a vector representing their relative rotation is generated in $(-30,\ 30)$(deg).

We analyzed three aspects of the proposed algorithm: performance for measurement noise, errors in orthogonality assumption of the two planes and the number of used frames. The experimental results are shown in Fig. 5. Gaussian noise $N(0, 30)$ is added to the range data used in Fig. 5(a). The angle between the two planes is changed from 85 to 95(deg) in Fig. 5(b) to demonstrate the performance of the proposed algorithm if the assumption of orthogonality is broken. The number of frames used for calibration is changed from 8 to 40 in Fig. 5(c) under the additive Gaussian noise of $N(0, 5)$ to the range data.

In the experiment, the initial and refined values of the extrinsic parameters computed by the proposed algorithm are compared to the ground truth. The difference in rotation is measured by the angle of the difference $\delta\mathbf{R}$ between the ture rotation $\mathbf{R}_{true}$ and the measured rotation $\mathbf{R}_{measured}$ as $\delta\mathbf{R} = \mathbf{R}_{true} * {\mathbf{R}_{measured}}^{-1}$. The angle of δR expressed in the angle-axis representation and the L_2 norm of translation are computed as rotation and translation errors, respectively.

In Fig. 5, we performed 100 trials and computed the mean and standard deviation of the rotation and translation errors. Blue and red lines indicate the performance of initial and refined results, respectively. As shown in Fig. 5(a) and (b), the rotation error of initial results increases smoothly as the noise increases. Fig. 5(b) shows that the proposed algorithm is very sensitive to the errors in the orthogonality of the two planes. The nonlinear optimization resolves this sensitivity issue because it optimizes the angle between the planes as well. Fig. 5(c) shows that changing frame numbers does not give much effect to the accuracy of the initial results. The red lines shows that the proposed optimization method reduces

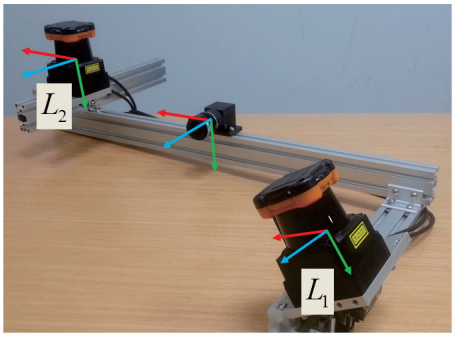

Fig. 6: Sensor configuration for real data experiment. Red, green and blue arrows denote **x**,**y** and **z** axes of each sensor coordinate system, respectively.

TABLE I: Estimated extrinsic parameters using real data

	Rotation (rad)
Conventional	-0.397912, -0.030092, -0.395114
Proposed	-0.383018, -0.009843, -0.369669
	Translation (mm)
Conventional	122.712734, -276.401163, -372.751889
Proposed	112.350861, -261.344662, -361.813052

the rotation error significantly in all cases. Fig. 5(d), (e) and (f) show the refined results in detail.

Translation errors are not displayed because their distribution is similar to that of the rotation errors.

B. Experiment using real data

For real-data experiments, we designed a sensor system which consists of two laser sensors (Hokuyo UTM-30LX) and a CCD camera (PointGrey Flea2) as shown in Fig. 6. Using real data, calibration result by the proposed method is compared to that by the conventional method with an extra camera by Zhang and Pless [8]. In order to compute the relative pose using the conventional method, the relative poses between the two laser sensors and the camera are multiplied; the extra camera "bridges" between the laser sensors.

Table I shows the results estimated by the proposed method and those by the conventional method. The rotation parameters are transformed into a 3×1 vector as mentioned in Sect. III-A. The rotation and translation differences between the conventional and the proposed method estimated as 0.909108 (deg) and 6.682265 (mm), respectively. The angle value θ between two planes is estimated to be 89.751313 (deg).

Fig. 7(a) shows the accumulated laser scan data on two planes from the two sensors L_1 (red) and L_2 (blue) with the estimated relative pose. The top-view shown in Fig. 7(b) verifies that the scan points in the world coordinate are on the two planes containing the y-axis, as we assumed, and it confirms that the proposed method successfully register the two laser sensors.

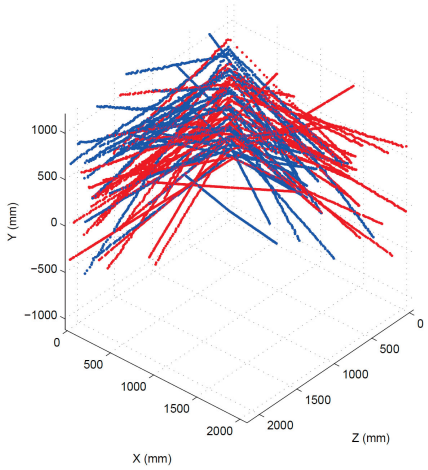

(a) Accumulated laser data

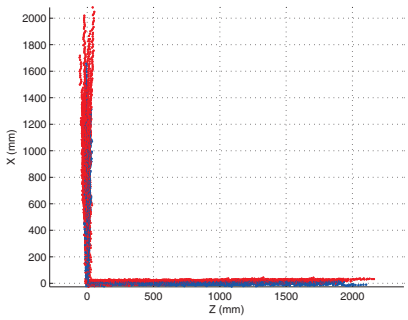

(b) Top view

Fig. 7: An example of accumulated laser data (red : L_1, blue : L_2) : (a) scanned laser data on two planes and (b) top view.

IV. CONCLUSIONS

In this paper, we present a novel method for extrinsic calibration of two 2D laser sensors. The proposed algorithm uses only range data scanned on two orthogonal planes without any additional sensor or information about motion of the laser sensors. Coplanarity of scan data from the two laser sensors gives a linear equation of their relative pose. Two 'mirrored' solutions are computed from the solution vector of the equation and its scale is determined by the orthogonality of two planes. We demonstrated the accuracy and robustness of the proposed algorithm using synthetic data with noise. The experiment using real data verifies that the proposed method provides a solution comparable to that of the conventional method, which uses an extra camera.

V. APPENDIX

1. Rotation parameters

$$r_{12} = \lambda v_1 = \lambda k_1$$
$$r_{21} = \lambda v_2 = \lambda k_2$$
$$r_{23} = \lambda v_3 = \lambda k_3$$
$$r_{32} = \lambda v_4 = \lambda k_4$$

$$r_{22} = \pm\sqrt{1 - \lambda^2(v_2^2 + v_3^2)} = \pm\sqrt{1 - \lambda^2 k_0}$$

$$r_{11} = \frac{-v_1 v_2 r_{22} \pm v_3 v_4}{v_1^2 + v_4^2} = -k_5 r_{22} \pm k_6$$
$$r_{31} = \frac{-v_2 v_4 r_{22} \mp v_1 v_3}{v_1^2 + v_4^2} = -k_7 r_{22} \mp k_8$$
$$r_{13} = \frac{-v_1 v_3 r_{22} \mp v_2 v_4}{v_1^2 + v_4^2} = -k_8 r_{22} \mp k_7$$
$$r_{33} = \frac{-v_3 v_4 r_{22} \pm v_1 v_2}{v_1^2 + v_4^2} = -k_6 r_{22} \pm k_5$$

2. Translation parameters

$$\begin{aligned} t_x &= \frac{\mp v_1(-v_3 v_7 + v_2 v_8) r_{22} + v_4(v_2 v_7 + v_3 v_8)}{v_4(v_2^2 + v_3^2)} \\ &= \mp k_{12} r_{22} + k_{13} \\ t_y &= \lambda \frac{(v_3 v_5 - v_2 v_6)}{\mp v_1} = \mp \lambda k_9 \\ t_z &= \frac{\pm v_4(v_3 v_5 - v_2 v_6) r_{22} - v_1(v_2 v_5 + v_3 v_6)}{v_1(v_2^2 + v_3^2)} \\ &= \pm k_{10} r_{22} - k_{11} \end{aligned}$$

3. k_n values

$$\begin{aligned} k_{14} &= -\Delta z_{21}(k_2 x'_3 + k_3 z'_3 \mp k_9) \\ k_{15} &= \Delta z_{21}(-k_1 x'_3 - k_4 z'_3 \mp k_{12}) \\ &\quad - \Delta x_{21}(-k_3 x'_3 - k_2 z'_3 \pm k_{10}) \\ k_{16} &= \Delta z_{21}(\pm k_2 x'_3 \mp k_3 z'_3 + k_{13} - x_1) \\ &\quad - \Delta x_{21}(\mp k_4 x'_3 \pm k_1 z'_3 - k_{11} - z_1) \\ k_{17} &= \Delta x_{21}(k_2 x'_3 + k_3 z'_3 \mp k_9) \\ k_{18} &= -\Delta z_{65}(k_2 x'_7 + k_3 z'_7 \mp k_9) \\ k_{19} &= \Delta z_{65}(-k_1 x'_7 - k_4 z'_7 \mp k_{12}) \\ &\quad - \Delta x_{65}(-k_3 x'_7 - k_2 z'_7 \pm k_{10}) \\ k_{20} &= \Delta z_{65}(\pm k_2 x'_7 \mp k_3 z'_7 + k_{13} - x_5) \\ &\quad - \Delta x_{65}(\mp k_4 x'_7 \pm k_1 z'_7 - k_{11} - z_5) \\ k_{21} &= \Delta x_{65}(k_2 x'_7 + k_3 z'_7 \mp k_9) \\ k_{22} &= k_{14} k_{18} + k_{17} k_{21} - k_{15} k_{19} k_0 \\ k_{23} &= k_{15} k_{20} + k_{16} k_{19} \\ k_{24} &= k_{15} k_{19} + k_{16} k_{20} \end{aligned}$$

The detailed derivation can be found in the supplementary material at `http://rcv.kaist.ac.kr/~dgchoi/icra2014derivation.pdf`

REFERENCES

[1] D. F. Wolf and G. S. Sukhatme, "Mobile robot simultaneous localization and mapping in dynamic environments," *Autonomous Robots*, vol. 19, no. 1, pp. 53–65, 2005.

[2] P. Newman, D. Cole, and K. Ho, "Outdoor slam using visual appearance and laser ranging," in *Robotics and Automation, 2006. ICRA 2006. Proceedings 2006 IEEE International Conference on*. IEEE, 2006, pp. 1180–1187.

[3] A. Nuchter, K. Lingemann, J. Hertzberg, and H. Surmann, "6d slam with approximate data association," in *Advanced Robotics, 2005. ICAR'05. Proceedings., 12th International Conference on*. IEEE, 2005, pp. 242–249.

[4] D. M. Cole and P. M. Newman, "Using laser range data for 3d slam in outdoor environments," in *Robotics and Automation, 2006. ICRA 2006. Proceedings 2006 IEEE International Conference on*. IEEE, 2006, pp. 1556–1563.

[5] S. Thrun, M. Montemerlo, H. Dahlkamp, D. Stavens, A. Aron, J. Diebel, P. Fong, J. Gale, M. Halpenny, G. Hoffmann, *et al.*, "Stanley: The robot that won the darpa grand challenge," *Journal of field Robotics*, vol. 23, no. 9, pp. 661–692, 2006.

[6] M. Montemerlo, J. Becker, S. Bhat, H. Dahlkamp, D. Dolgov, S. Ettinger, D. Haehnel, T. Hilden, G. Hoffmann, B. Huhnke, *et al.*, "Junior: The stanford entry in the urban challenge," *Journal of Field Robotics*, vol. 25, no. 9, pp. 569–597, 2008.

[7] Y. Bok, Y. Jeong, D.-G. Choi, and I. S. Kweon, "Capturing village-level heritages with a hand-held camera-laser fusion sensor," *International Journal of Computer Vision*, vol. 94, no. 1, pp. 36–53, 2011.

[8] Q. Zhang and R. Pless, "Extrinsic calibration of a camera and laser range finder (improves camera calibration)," in *Intelligent Robots and Systems, 2004.(IROS 2004). Proceedings. 2004 IEEE/RSJ International Conference on*, vol. 3. IEEE, 2004, pp. 2301–2306.

[9] J. Underwood, A. Hill, and S. Scheding, "Calibration of range sensor pose on mobile platforms," in *Intelligent Robots and Systems, 2007. IROS 2007. IEEE/RSJ International Conference on*. IEEE, 2007, pp. 3866–3871.

[10] C. Gao and J. R. Spletzer, "On-line calibration of multiple lidars on a mobile vehicle platform," in *Robotics and Automation (ICRA), 2010 IEEE International Conference on*. IEEE, 2010, pp. 279–284.

[11] W. Maddern, A. Harrison, and P. Newman, "Lost in translation (and rotation): Rapid extrinsic calibration for 2d and 3d lidars," in *Robotics and Automation (ICRA), 2012 IEEE International Conference on*. IEEE, 2012, pp. 3096–3102.

[12] J. Levinson and S. Thrun, "Unsupervised calibration for multi-beam lasers," in *Experimental Robotics*. Springer, 2014, pp. 179–193.